NeuroImage 194 (2019) 291–302

Contents lists available at ScienceDirect

NeuroImage

journal homepage: www.elsevier.com/locate/neuroimage

Phase-matched virtual coil reconstruction for highly accelerated diffusion echo-planar imaging

Congyu Liao [a,b,c], Mary Kate Manhard [a,b], Berkin Bilgic [a,b], Qiyuan Tian [a,b], Qiuyun Fan [a,b], Sohyun Han [a,b], Fuyixue Wang [d], Daniel Joseph Park [a], Thomas Witzel [a,b], Jianhui Zhong [c], Haifeng Wang [a,b,e,*], Lawrence L. Wald [a,b], Kawin Setsompop [a,b]

[a] Athinoula A. Martinos Center for Biomedical Imaging, Massachusetts General Hospital, Charlestown, MA, USA
[b] Department of Radiology, Harvard Medical School, Boston, MA, USA
[c] Center for Brain Imaging Science and Technology, Key Laboratory for Biomedical Engineering of Ministry of Education, College of Biomedical Engineering and Instrumental Science, Zhejiang University, Hangzhou, Zhejiang, China
[d] Harvard-MIT Health Sciences and Technology, MIT, Cambridge, MA, USA
[e] Paul C. Lauterbur Research Centre for Biomedical Imaging, Shenzhen Institute of Advanced Technology, Chinese Academy of Science, Shenzhen, Guangdong, China

ARTICLE INFO

Keywords:
Virtual coil
Single-shot EPI
gSlider
Diffusion imaging

ABSTRACT

Purpose: To propose a virtual coil (VC) acquisition/reconstruction framework to improve highly accelerated single-shot EPI (SS-EPI) and generalized slice dithered enhanced resolution (gSlider) acquisition in high-resolution diffusion imaging (DI).

Methods: For robust VC-GRAPPA reconstruction, a background phase correction scheme was developed to match the image phase of the reference data with the corrupted phase of the accelerated diffusion-weighted data, where the corrupted phase of the diffusion data varies from shot to shot. A G_y prewinding-blip was also added to the EPI acquisition, to create a shifted-k_y sampling strategy that allows for better exploitation of VC concept in the reconstruction. To evaluate the performance of the proposed methods, 1.5 mm isotropic whole-brain SS-EPI and 860 μm isotropic whole-brain gSlider-EPI diffusion data were acquired at an acceleration of 8–9 fold. Conventional and VC-GRAPPA reconstructions were performed and compared, and corresponding g-factors were calculated.

Results: The proposed VC reconstruction substantially improves the image quality of both SS-EPI and gSlider-EPI, with reduced g-factor noise and reconstruction artifacts when compared to the conventional method. This has enabled high-quality low-noise diffusion imaging to be performed at 8–9 fold acceleration.

Conclusions: The proposed VC acquisition/reconstruction framework improves the reconstruction of DI at high accelerations. The ability to now employ such high accelerations will allow DI with EPI at reduced distortion and faster scan time, which should be beneficial for many clinical and neuroscience applications.

1. Introduction

Diffusion imaging (DI) is a noninvasive technique that can probe tissue microstructure by applying diffusion encoding gradients. DI is widely used in many clinical and neuroscience applications, with rapid Echo Planer Imaging (EPI) being the acquisition technique of choice as it allows imaging at a large number of diffusion encodings in an acceptable timeframe. The single-shot variant of EPI (SS-EPI) which acquires the entire k-space data in a single TR is the most commonly used approach, because of its fast acquisition and its immunity to bulk motion. However, the associated lengthy echo train of SS-EPI induces T_2* blurring and B_0 distortion, imposing a limitation on achievable resolution (Constable and Gore, 1992). The development of parallel imaging techniques over the years has helped to improve the quality of DI that can be obtained from SS-EPI. In particular, in-plane acceleration methods (Bammer et al., 2001; Gao et al., 2014; Wen et al., 2018; Xie et al., 2018) have helped mitigate distortion (Blaimer et al., 2004) and blurring, while simultaneous multislice (SMS) techniques (Setsompop et al., 2012b) exciting

* Corresponding author. Paul C. Lauterbur Research Centre for Biomedical Imaging, Shenzhen Institute of Advanced Technology, Chinese Academy of Science, Shenzhen, Guangdong, China.
E-mail address: hf.wang1@siat.ac.cn (H. Wang).

https://doi.org/10.1016/j.neuroimage.2019.04.002
Received 16 November 2018; Received in revised form 26 March 2019; Accepted 1 April 2019
Available online 3 April 2019
1053-8119/© 2019 Published by Elsevier Inc.

multi-band (MB) slices simultaneously have shortened the TR and therefore helped to accelerate all types of EPI acquisitions. Nonetheless, the total achievable acceleration with parallel imaging is typically limited to 4–6 fold (e.g. $R_{inplane} \times MB = 2 \times 2$) (Fan et al., 2017; Setsompop et al., 2012a), even with the use of high channel count receiver arrays (e.g. 32 channels). At higher accelerations, significant g-factor noise amplification and image artifacts start to become problematic in DI.

Multi-shot EPI (MS-EPI) acquisition strategies including readout segmented EPI (Porter and Heidemann, 2009), interleaved EPI with total variation constraint (Chen et al., 2013) and dual spin-echo EPI with a 2D navigator (Jeong et al., 2013) are promising approaches for high-resolution diffusion imaging as it allows for shorter effective echo spacing to mitigate distortion and blurring. However, lengthy scan times and sensitivity to shot-to-shot phase and motion variations are key challenges in DI with MS-EPI (Anderson and Gore, 1994). A number of approaches based on SMS (Chang et al., 2015; Dai et al., 2017), parallel imaging (Hu et al., 2017; Zhang et al., 2015) with sparsity (Mani et al., 2015; Shi et al., 2015) or low rank models (Haldar, 2014; Hu et al., 2018; Liao et al., 2017; Mani et al., 2017), joint reconstruction (Bilgic et al., 2018; Haldar et al., 2013) and partial Fourier reconstruction (Guo et al., 2016) were proposed to shorten the total acquisition time and correct for shot-to-shot phase variations. In particular, the MUSE technique (Chen et al., 2013) introduced an approach to estimate phase differences in multi-shot EPI and incorporate that information into the joint reconstruction of multi-shot data.

To further accelerate DI, smooth phase prior or conjugate property of k-space can be utilized as prior information for reconstruction. As a commonly used method, partial Fourier techniques (Cuppen and van Est, 1987; Haacke et al., 1991; Noll et al., 1991) that reduce sampling lines on one side of k-space can efficiently shorten the echo time (TE) and thereby improve the SNR in DI. However, such approaches do not reduce echo spacing and hence distortion/blurring.

The virtual coil (VC) concept (Blaimer et al., 2009) is another approach that utilizes smooth phase prior. In this case, the virtual coils containing conjugate symmetric k-space signals are generated from actual coils, and the effective doubled channels with additional phase information can be incorporated into the process of standard GRAPPA reconstruction to improve the performance of reconstruction, which has been demonstrated to enable higher in-plane and/or MB accelerations in a number of applications (Blaimer et al., 2014, 2013; Kettinger et al., 2018; Schneider et al., 2012). For EPI acquisitions, this allows for reduced distortion and improved speed (albeit with less TE reduction when compared to partial Fourier). Nonetheless, its usage in DI has been restricted by the shot-to-shot background phase variations, which violate VC phase prior assumption. The phase variation is a key challenge in DI. Here we estimate the phase corruption and incorporate this information as a prior information to improve the parallel imaging reconstruction performance of highly accelerated single-shot EPI data.

In this work, we proposed a new 'phase-matched' VC-GRAPPA reconstruction framework and demonstrate its utility in achieving high quality reconstruction for 9-fold accelerated DI data ($MB \times R_{in\text{-}plane} = 3 \times 3$), comparing the proposed framekwork to the conventional VC-GRAPPA reconstruction. The phase matching processing was proposed to incorporate the shot-to-shot phase variations into the reference data of VC-GRAPPA while ensuring that it is not corrupting the ACS data. Furthermore, a shifted-k_y acquisition strategy was also implemented to further improve VC reconstruction. In addition, we applied this method in our recently proposed generalized slice dithered enhanced resolution (gSlider) acquisition (Setsompop et al., 2018) to achieve efficient sub-millimeter DI with 8-fold acceleration ($MB \times R_{inplane} = 2 \times 4$). gSlider is an SNR-efficient simultaneous multi-slab acquisition that utilizes a novel RF slab-encoding to enable self-navigation of diffusion phase corruption and motion robustness (Wang et al., 2018a). The results demonstrate that the proposed VC method for DI enables higher accelerations with reduced g-factor penalty and better reconstruction when compared to the conventional method.

2. Methods

2.1. Shifted k_y & k_z sampling strategy

Fig. 1(a) shows the sequence diagram of the SS-EPI used in this work for SMS and gSlider acquisitions. Slice-fully-sampled single-shot spin-echo EPI was used as the reference data for SMS acceleration and fully sampled fast low-angle excitation echo-planar technique (FLEET) sequence (Polimeni et al., 2016) was used as the reference for in-plane acceleration. The FLEET sequence is applied to reorder the segments of the in-plane reference data so that segments within any given slice are acquired consecutively in time, which can reduce the sensitivity loss due to respiration and bulk motion in accelerated EPI acquisitions. Additionally, a G_y prewinding-blip is added prior to the EPI train, to generateΔk_y shifts in the acquired data (or linear phase ramp in image domain) (Fig. 1(b)). The benefit of such a Δk_y shift is to provide more unique k-space source points for VC reconstructions. For data acquired with '$R_{inplane}$' acceleration factor and a shift of Δk_y, the k_y lines at positions: { … $\Delta k_y + R_{inplane}$, Δk_y,Δk_y-$R_{inplane}$ … } are acquired. When VC reconstruction is used through conjugate virtual coil, the k_y lines at positions { …, -Δk_y+$R_{inplane}$, -Δk_y, -Δk_y-$R_{inplane}$ … } are synthesized. To maximize the effectiveness of VC reconstruction, a uniform gap between different synthesized lines is desired to help minimize the maximum k-space gap in the data. Therefore, a Δk_y shift of $R_{inplane}/4$ is the optimal factor since it will create the same spacing of $R_{inplane}/2$ across the synthesized k-space lines. In this study, Δk_y shifts of 0.75 and 1.00 line were applied for $R_{in\text{-}plane} = 3$ and $R_{in\text{-}plane} = 4$, respectively.

Similar to the Δk_y shift, a G_z prewinding blip can be added in slice-selection dimension to generate Δk_z shifts in k_y-k_z space (Blaimer et al., 2013). In this study since a FOV/2 shift between SMS slices was created by blipped-CAIPI with G_z blips, the acquired k-space points along k_z are asymmetric. Therefore the additional G_z blips are not necessary in the blipped-CAIPI acquisition with FOV/2 controlled-aliasing shift case.

2.2. VC reconstruction

Due to shot-to-shot background phase variations in DI, the image phase of each under-sampled diffusion weighted EPI will differ significantly from one another and from the fully-sampled reference data. As such, VC-GRAPPA reconstruction trained on the reference data cannot be applied directly to the under-sampled data without causing severe artifacts, and a phase matching process between under-sampled data and reference data is needed. Fig. 2 shows the flowchart of the proposed phase-matched VC reconstruction for DI data acquired with in-plane and slice accelerations, which includes following steps:

(i) **Conventional reconstruction:** The accelerated EPI data were first reconstructed using slice-GRAPPA (Setsompop et al., 2012a) followed by in-plane GRAPPA (Griswold et al., 2002) (Fig. 2(a)). Leak-block slice-GRAPPA algorithm (Cauley et al., 2014) was employed to improve reconstruction, and the dual-kernel and two-step ghost correction were used to minimize Nyquist ghosting artifacts (Setsompop et al., 2012a). Slice-fully-sampled single-shot spin-echo EPI was used as the reference data of SMS acceleration and fully sampled multi-shot FLEET sequence was used as the reference of in-plane GRAPPA acceleration to achieve robustness against motion (Fig. 1(a)).

(ii) Background phase matching: The aim of the phase matching process is to match the image phase of the reference data to the varied phase of the diffusion data so that correct phase prior is used in the VC-GRAPPA reconstruction. To provide the correct phase, the image phase of conventionally reconstructed diffusion data can be used to replace the image phase of the reference data on a coil-by-coil basis for the VC-GRAPPA kernel fitting. However, the phases of these individual coil images are likely to be very noisy and contain significant artifacts from the conventional reconstruction at high accelerations.

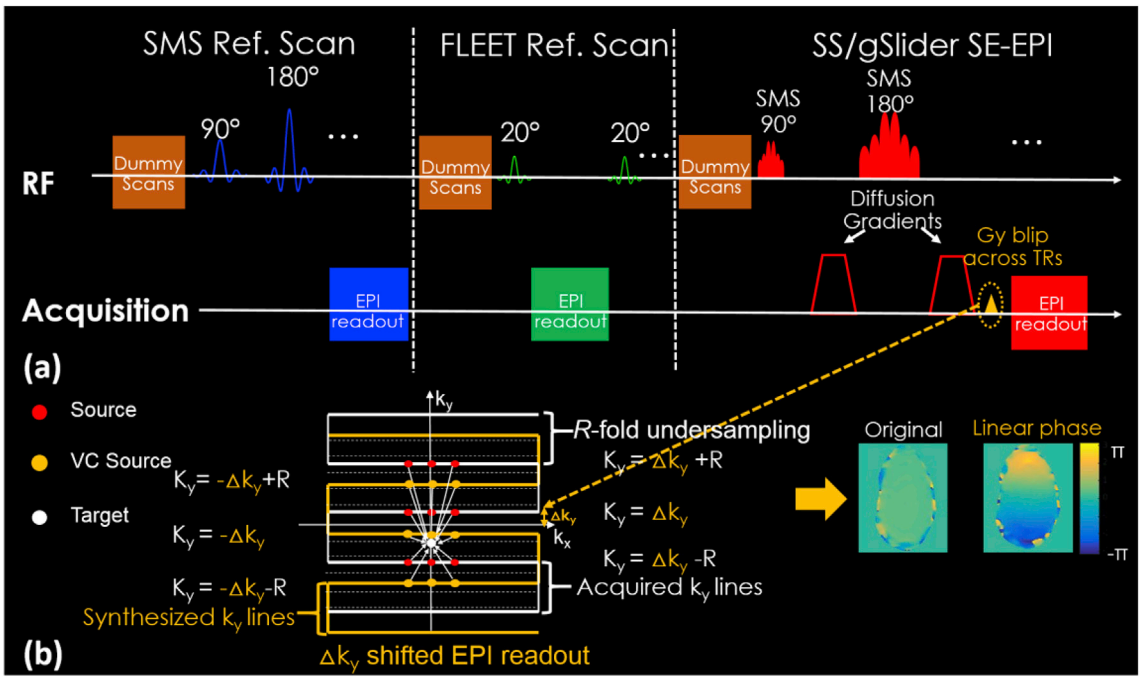

Fig. 1. (a) The sequence diagram of EPI acquisition with additional G_y blips across TRs (marked in yellow, located in the right portion of the sub-figure). The SMS reference data are acquired by SE-EPI, the in-plane reference data are acquired by FLEET scan and the undersampled data are acquired by single-shot (SS) or gSlider SE-EPI scans. (b) The shifted k_y lines generate a linear ramp phase in the image domain, which improves VC-GRAPPA reconstruction.

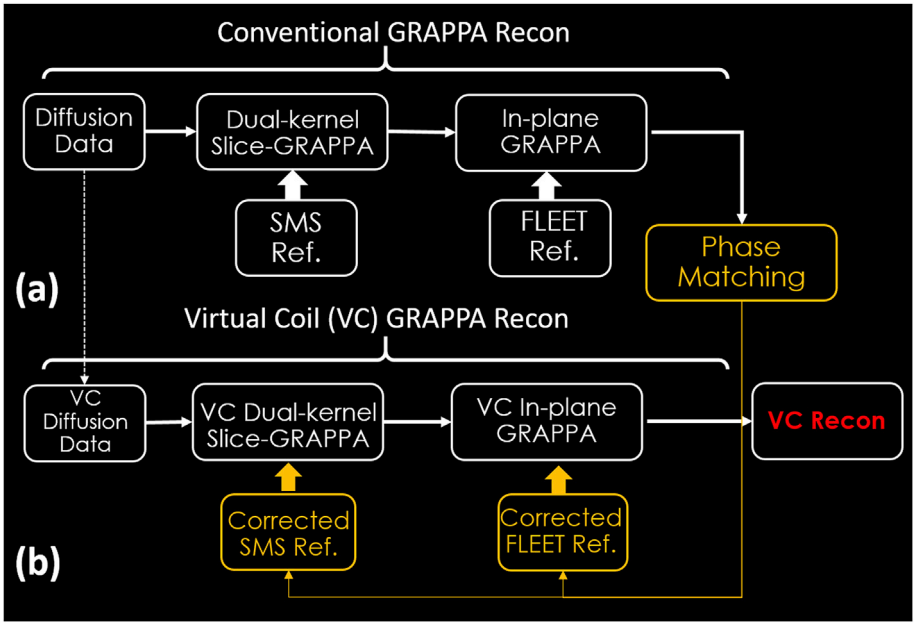

Fig. 2. The flowchart of (a) conventional and (b) VC reconstruction.

To provide a better phase estimate, the procedure outlined in Fig. 3(a) is proposed. First, the image phase difference between conventionally reconstructed diffusion data and SMS reference data is calculated. This calculation is performed on the complex-coil-combined image rather than on a coil-by-coil basis to achieve good SNR (phase difference should be the same across coils). Since the phase differences should also be relatively smooth, given that they originated from the interaction of motion and diffusion encoding gradients, the estimated phase differences were filtered by a 2D Hamming window to further remove noise. The filtered phase was then added to the coils' phases of the SMS reference data, to generate a phase-matched reference data for VC slice-GRAPPA fitting. For the gradient-echo based FLEET reference data used in the in-plane GRAPPA fitting, the image phase contains large phase wraps and will also differ significantly from the diffusion data. Instead of calculating the phase difference again in the FLEET data, the phase from the phase-matched SMS reference data was used to replace the phase of FLEET reference data, coil-by-coil, to create a phase-matched reference data for VC in-plane-GRAPPA fitting. Fig. 3(b) shows the comparison of the conventional reconstruction, VC-GRAPPA reconstruction without phase matching, and

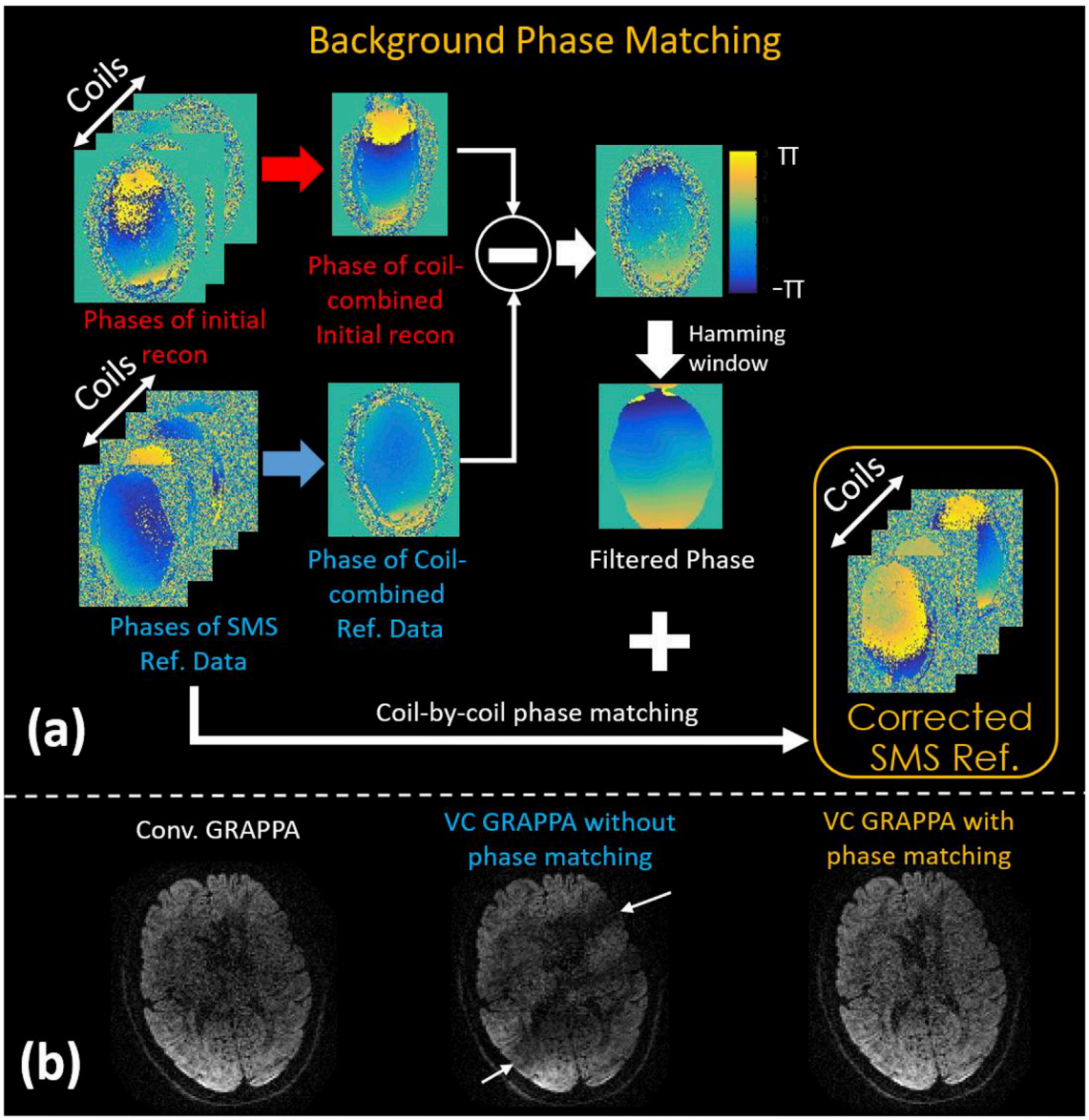

Fig. 3. The flowchart of background phase matching method. The phase maps of the reference data are updated after Hamming filtering to generate unique VC-GRAPPA kernels to reconstruct data for each diffusion direction.

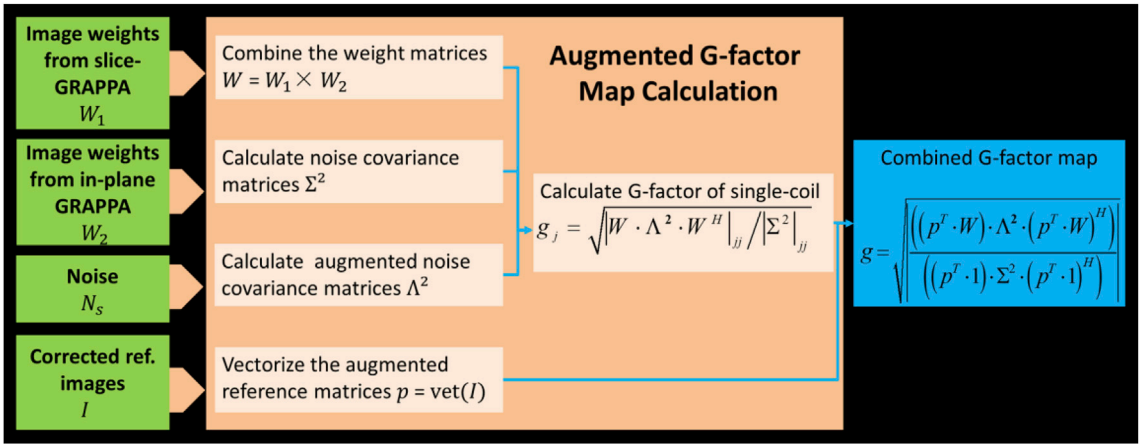

Fig. 4. The flowchart of g-factor map calculation.

VC-GRAPPA reconstruction with phase matching. As indicated by the white arrow, direct application of VC reconstruction without background phase matching causes severe artifacts due to the dramatically phase variation between the diffusion data and the reference data.

(iii) VC reconstruction: Fig. 2(b) shows the flowchart of VC reconstruction, where additional virtual coil data were generated through complex conjugation of the under-sampled diffusion data. The data were then reconstructed again using VC slice- and in-plane GRAPPA. A set of VC-GRAPPA kernel weights was estimated from the phase-matched reference data, which contains the specific background phase of the diffusion weighted acquisition to be reconstructed.

2.3. Augmented g-factor calculation

To characterize the performance of our VC reconstruction approach, g-factor maps were calculated pixel-by-pixel from the image weights of GRAPPA kernels and the noise correlations of coils, which can be derived from an additional noise pre-scan. Fig. 4 shows the procedure of the g-factor calculation. The image weights of the dual-kernel slice-GRAPPA (W_1) were synthesized from the odd and even slice-GRAPPA kernel weights using the method from (Wang et al., 2017) and the image weights of in-plane GRAPPA (W_2) were estimated from the in-plane GRAPPA kernels (Breuer et al., 2009; Wang et al., 2005). The final image weights were combined pixel-by-pixel by multiplication of slice- and in-plane GRAPPA matrices $W = W_1 \times W_2$.

We define the pre-scan noise matrix of all M coils as Ns, thereby the noise covariance matrix of all coils Σ^2 can be calculated. For VC reconstruction, since the noise distribution of the virtual coils has the same standard deviations and mean values as the real coils, and the noise correlations between real and virtual coils is 0, the augmented noise covariance matrix of VC reconstruction Λ^2 can be extended to:

$$\Lambda^2 = \begin{bmatrix} \Sigma^2 & 0 \\ 0 & \Sigma^2 \end{bmatrix}_{2M\times 2M}. \quad (1)$$

Therefore, the g-factor of a single coil (i.e., jth coil) is calculated by:

$$g_j = \sqrt{\left|W \cdot \Lambda^2 \cdot W^H\right|_{jj} \Big/ \left|\Sigma^2\right|_{jj}}. \quad (2)$$

and the coil-combined g-factor map can be derived as (Wang et al., 2017):

$$g_{comb} = \sqrt{\left|\frac{\left((p^T \cdot W) \cdot \Lambda^2 \cdot (p^T \cdot W)^H\right)}{\left((p^T \cdot 1) \cdot \Sigma^2 \cdot (p^T \cdot 1)^H\right)}\right|}. \quad (3)$$

Similar to the coil combination method in (Breuer et al., 2009), the coil sensitivity value p_j in the vector $\mathbf{p}$ can be determined from the phase-corrected reference data (note that the virtual-coil sensitivities are set as zero since the final results of VC reconstruction only utilizes the real-coil part).

2.4. In vivo data acquisition

All in vivo measurements were performed on a 3T scanner (MAGNETOM Prisma, Siemens Healthineers, Erlangen, Germany). Whole-brain DI data were acquired in 4 volunteers at 1.5 mm isotropic using a single-shot SMS-EPI sequence with a 32-channel head coil. The acceleration factors were $MB \times R_{inplane} = 3 \times 3$, with a k_y-shift of 0.75 to maximize the utility of phase priors. A FOV/2 controlled-aliasing shift between SMS slices was created using blipped-CAIPI scheme with the standard prewinding kz blip of $-\pi/2$ to ensure the k_z sampling during the EPI readout is centered at $kz = 0$. The imaging parameters were: FOV = 220 × 220 × 139 mm^3, the effective echo spacing = 0.65/3 ms = 0.217 ms (due to $R_{inplane} = 3$), 64 diffusion-directions at b = 1000 s/mm^2 with one b = 0 image, and TE/TR = 69 ms/3.3s. The total acquisition time of one average was ~4.5 min. To obtain high-SNR FA maps, three averages were acquired, corresponding to a total acquisition time of 13.5 min.

We also applied the VC reconstruction framework to our recently proposed gSlider-EPI, to achieve high-SNR high-resolution DI at a high acceleration. Whole-brain 0.86 mm isotropic data were acquired using gSlider-EPI with a 64-channel Siemens head-neck coil. In this study, we only used 52-channel head elements for brain imaging. The acceleration factors were $MB \times R_{inplane} = 2 \times 4$ with k_y-shift set to 1, and with blipped-CAIPI shift of FOV/2. A gSlider RF-encoding of 5 was used, which when combined with the MB acceleration of 2 achieves 10 simultaneous slices per shot acquisition to provide good SNR efficiency for this submillimeter isotropic acquisition. The FOV of the acquisition was 220 × 220 × 146 mm^3, the effective echo spacing = 0.97/4 ms = 0.242 ms. A total of 34 thin-slab (4.3 mm-slabs) were acquired per gSlider RF-encoding, with 5 RF-encodings acquired consecutively and combined to reconstruct 0.86 mm slices. Both 30 and 64 diffusion-directions with b = 1000 s/mm^2 were acquired at TE/TR = 91 ms/3.5s. The total acquisition of 30 and 64 diffusion-directions were ~9 and 20 min, respectively. For accurate gSlider reconstruction, the RF encoding basis used in the reconstruction were obtained from a Bloch simulation that accounts for B_1^+ inhomogeneity (an extra 10 s B_1^+ was scanned before gSlider acquisition) and spin-history effect of short-TR acquisition at 3.5s (assuming average T1 value of 1s) (Liao et al., 2018).

The reconstruction algorithms were implemented in MATLAB R2014a (The MathWorks, Inc., Natick, MA). To achieve faster GRAPPA reconstruction, SVD coil compression (Buehrer et al., 2007) was applied to compress 32 channel coil to 20 channels and 52 channel coil to 32 channels, respectively. SMS-EPI and gSlider-EPI data were reconstructed using both the conventional and VC-GRAPPA methods. Real-valued diffusion processing (Eichner et al., 2015) was applied for unbiased signal averaging to eliminate shot-to-shot background phase variations of complex-valued diffusion data. The FA maps of single-shot SMS-EPI were then fitted using the real-valued diffusion data with motion and eddy-current correction, where the FSL toolbox (Jenkinson et al., 2012) (https://fsl.fmrib.ox.ac.uk/fsl/fslwiki/) was utilized for the diffusion post-processing pipeline.

3. Results

Fig. 5 shows a comparison of GRAPPA vs. VC-GRAPPA reconstructions across a representative slice-group of three simultaneously excited slices from the 1.5 mm isotropic SS-EPI dataset at $MB \times R_{inplane} = 3 \times 3$. Reconstructed data from both b = 0 and b = 1000 s/mm^2 volumes are shown along with the corresponding 1/g-factor maps. For the b = 0 data, the g-factor noise is significantly higher with conventional GRAPPA when compared to VC-GRAPPA, with G_{avg} and G_{max} being 29% and 37% higher respectively (1.51 vs. 1.17, and 2.03 vs. 1.48). Similar g-factor results were obtained in the b = 1000 dataset, with g-factor from VC-GRAPPA being marginally higher than in the b = 0 case, due to the added image phase of this diffusion weighted acquisition. As can be seen, the image reconstruction performance also improved with VC-GRAPPA.

Fig. 6 shows three orthogonal views of a representative diffusion weighted volume from this dataset, which clearly demonstrate the improved reconstruction quality through VC-GRAPPA, where the undesirable dark patches at the center of images in the conventional reconstruction at this high acceleration is nicely mitigated. The white arrows in Figs. 5 and 6 highlight image structures that were successfully recovered through VC-GRAPPA reconstruction.

Fig. 7(a) shows a comparison of GRAPPA and VC-GRAPPA reconstructions across five different diffusion directions, where each acquisition experiences a different background phase corruption. Since a different background phase prior was used in VC-GRAPPA of each diffusion direction, the g-factor of VC-GRAPPA varies across directions while the g-factor of conventional GRAPPA reconstruction remains constant ($G_{avg} = 1.46$). Nonetheless, the g-factor of VC-GRAPPA remains

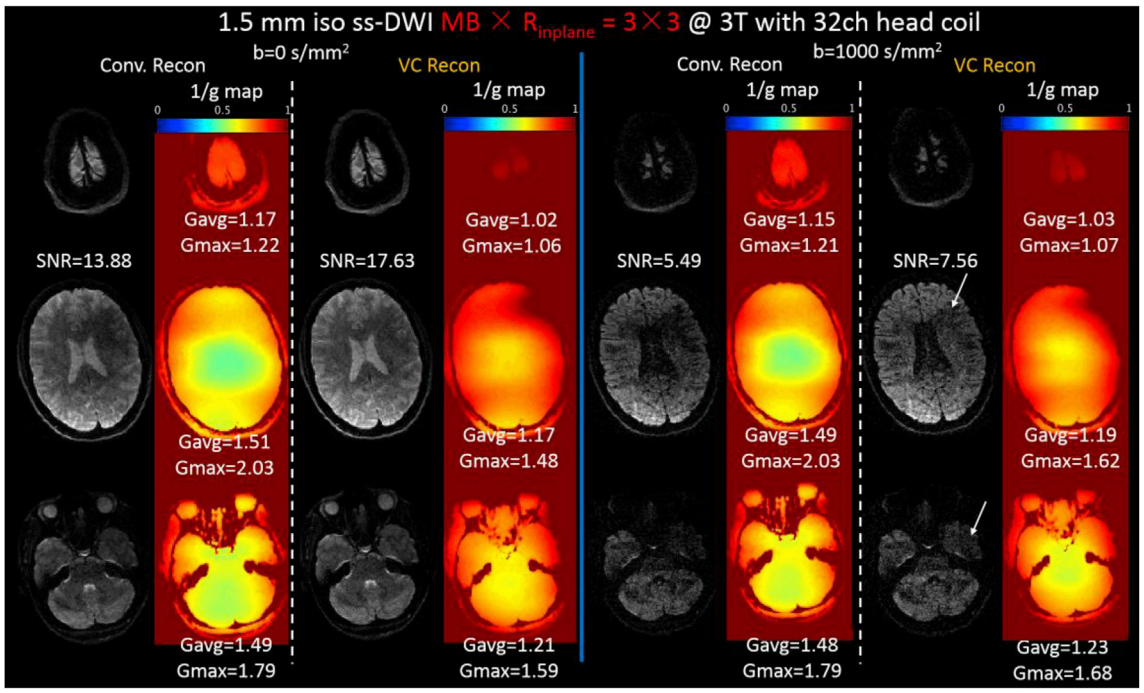

Fig. 5. Reconstructions and 1/g-factor maps of a slice group of diffusion imaging data with b = 0 and 1000 s/mm^2, respectively. The white arrows indicate that the artifacts in conventional method were recovered by VC reconstruction.

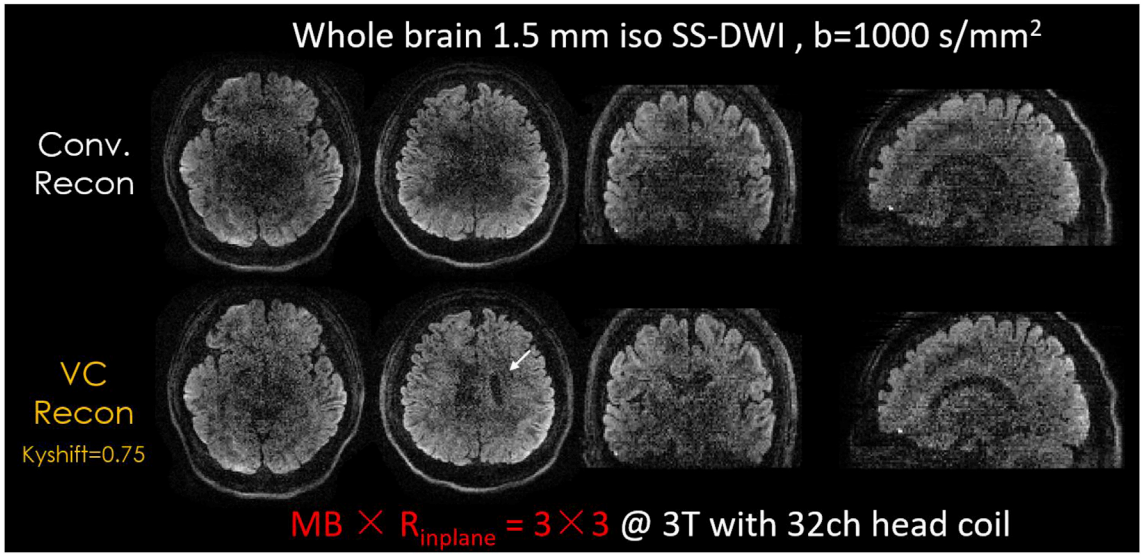

Fig. 6. Reconstructions of whole-brain 1.5 mm^3 diffusion imaging data, acquired with $R_{inplane} \times MB = 3 \times 3$. Artifacts in conventional GRAPPA reconstruction are mitigated through VC-GRAPPA (highlighted by white arrows). A k_y-shift of 0.75 was used in the acquisition to help maximize the utility of phase prior in VC-GRAPPA reconstruction.

consistently lower than that of conventional GRAPPA as expected, with the average and maximum g-factors of conventional GRAPPA being ~20% and 13% higher than the averaged g-factor values of VC-GRAPPA across directions. Moreover, significant artifact reductions are also observed with VC-GRAPPA (white arrows). Fig. 7(b) shows the 1/g-factor maps of conventional reconstruction, VC-GRAPPA with and without k_y shifts. As can be seen, the reconstruction performance of VC-GRAPPA is improved with the shift-k_y sampling strategy. Fig. 7(c) shows the comparison of conventional reconstruction, VC-GRAPPA with and without k_y shift for one diffusion direction with 5 repetitions. Since the background phase varies across repetitions, the "dark area" and the reconstructions of each repetition are different. As shown in Fig. 7(c), VC-GRAPPA with k_y shift shows the best reconstruction performance and the highest SNR among these three methods, which has demonstrated that the proposed k_y shift acquisition strategy could further improve the VC reconstruction.

Fig. 8 shows three orthogonal views of (a) 64-direction averaged-DWIs and (b) colored-FA maps obtained from conventional and VC-GRAPPA reconstructions of the 1.5 mm isotropic data, with three data averaging and total acquisition time of 13.5 min. The averaged-DWI and FA-map were improved through VC-GRAPPA, with substantial reduction in artifacts and noise for this 9-fold accelerated acquisition. The zoomed-in windows of the FA maps show that conventionally reconstructed data has significant residual artifacts that are leaking through in the resulting

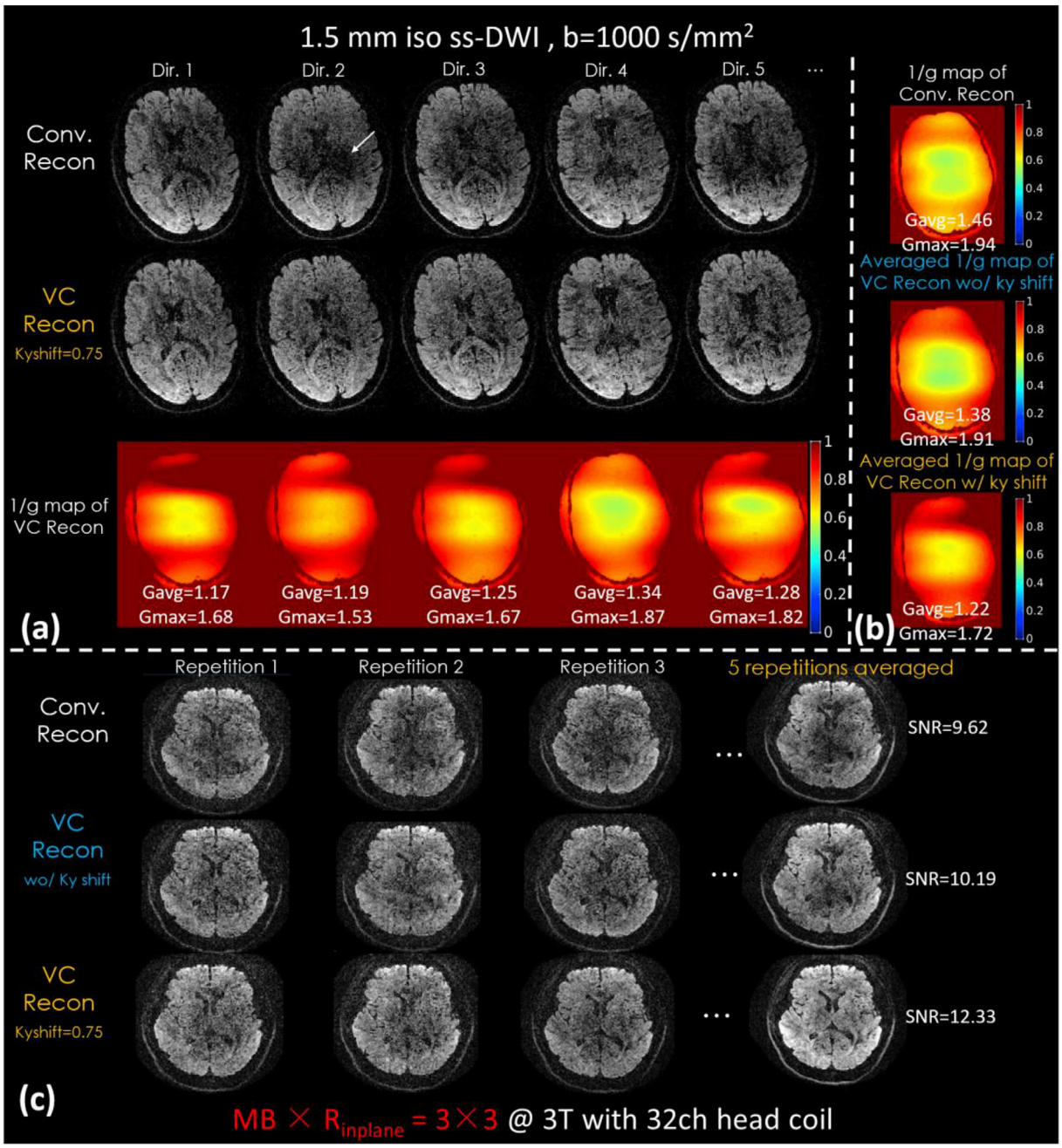

Fig. 7. (a) Reconstructions and 1/g-factor maps of a slice with five diffusion directions. (b) The averaged 1/g-factor map of VC reconstruction is compared with conventional method. (c) The comparison of conventional reconstruction, VC-GRAPPA with and without k_y shift for one diffusion direction with 5 repetitions.

FA map, while the VC reconstruction cleans this up nicely and also provides lower noise.

Fig. 9 shows the conventional and VC-GRAPPA reconstruction of 860 μm isotropic gSlider data at $MB \times R_{inplane} \times gSlider = 2 \times 4 \times 5$, where (a) shows the reconstructed RF-encoded thin-slabs (2 out of 5 shown) and the corresponding 1/g factor maps with in-plane resolution of $0.86 \times 0.86\ mm^2$, and (b) shows representative 2 of 5 resolved slices of 30 diffusion-directions averaged DWIs at 0.86 mm slice thickness. Sagittal and coronal views of the whole-brain averaged DWIs are also shown in Fig. 9(b). The 1/g factor maps show that the g-factor of conventional reconstruction across different RF-encodings are consistent, while the VC-GRAPPA reconstruction improve the g-factor, with G_{avg} and G_{max} being 16% and 6.8% lower respectively (1.50 vs. 1.29, and 2.02 vs. 1.89). In Fig. 9(b) the reconstructions of 860 μm isotropic diffusion data also showed that using k_y-shifted acquisition across slab-encoding improves VC reconstruction quality without smoothing away structural differences that exist across the slices within each slab.

Three orthogonal views of (a) 64 diffusion-direction averaged-DWIs and (b) colored-FA maps obtained from conventional and VC-GRAPPA reconstructions of the 860 μm isotropic data with one average at $MB \times R_{inplane} \times gSlider = 2 \times 4 \times 5$ are shown in Fig. 10. The zoomed-in figure highlights the ability of the visualization of cortical diffusion pattern in this high isotropic resolution data. The figure demonstrates that the VC-GRAPPA reconstruction enables high-quality averaged DWIs and FA maps at highly accelerated sub-millimeter resolution diffusion acquisition on a clinical 3T scanner.

4. Discussion

In this work, a phase-matched VC-GRAPPA reconstruction was

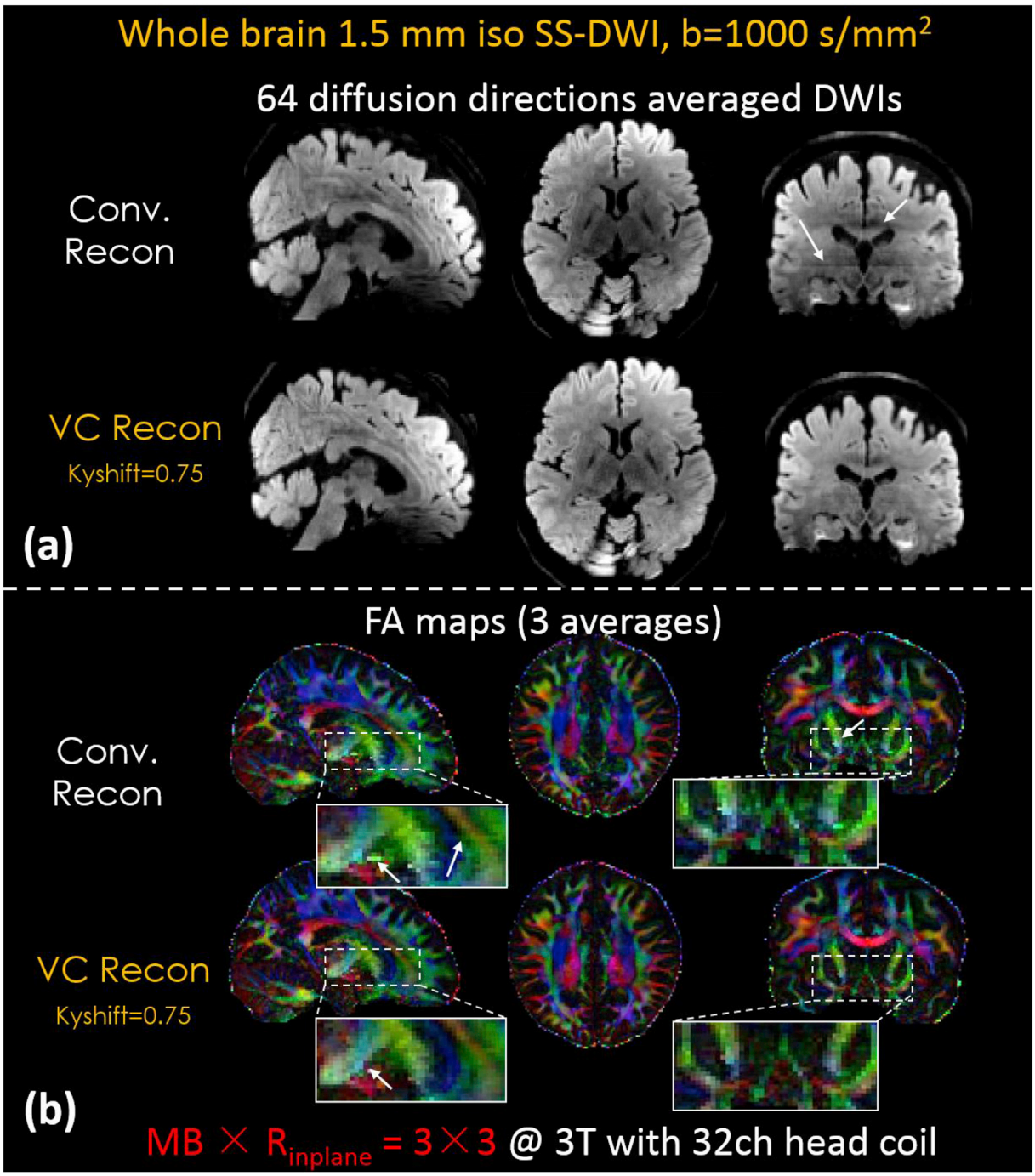

Fig. 8. Conventional and VC-GRAPPA reconstructions of (a) 64-direction averaged DWIs and (b) FA maps with three averages. The zoom-in windows of FA maps demonstrate that VC-GRAPPA provides significant reduction in artifacts and g-factor noise for this 9-fold accelerated acquisition.

proposed and demonstrated to achieve high-quality reconstruction for high-resolution diffusion imaging at 8–9 fold acceleration. Compared to the conventional method, VC reconstruction provides significant (~20%) reduction in g-factor penalty as well as improved reconstruction with much less artifacts. This enables the possibility of acquiring high-resolution diffusion imaging efficiently with low-distortion and artifacts. A shifted-k_y EPI sampling strategy was also used to better take advantage of the smooth-phase prior information in the reconstruction to provide 13% g-factor improvement over a non-shifted acquisition. We note that the proposed phase-matched VC and shifted-k_y EPI approaches are not only applicable to GRAPPA-based reconstruction, but should also be easily incorporated and extended to SENSE-based single- and multi-shot diffusion reconstruction such as MUSE (Chen et al., 2013), and readout segmented EPI (Porter and Heidemann, 2009), to effectively double the number of coil channels for the reconstruction.

The striping artifacts along the slice dimension are caused by the varied background phases of diffusion imaging and the ill-conditioning of the standard reconstruction at high acceleration. At high accelerations, standard reconstruction resulted in significant residual aliasing artifacts. With the background phase of the diffusion data changing from shot-to-shot and hence from slice-to-slice, the way the residual aliasing artifacts add or subtract from the data of one slice to another can change significantly, causing strong variation from slice to slice that shows up as striping artifacts. With the improvement in the conditioning of the

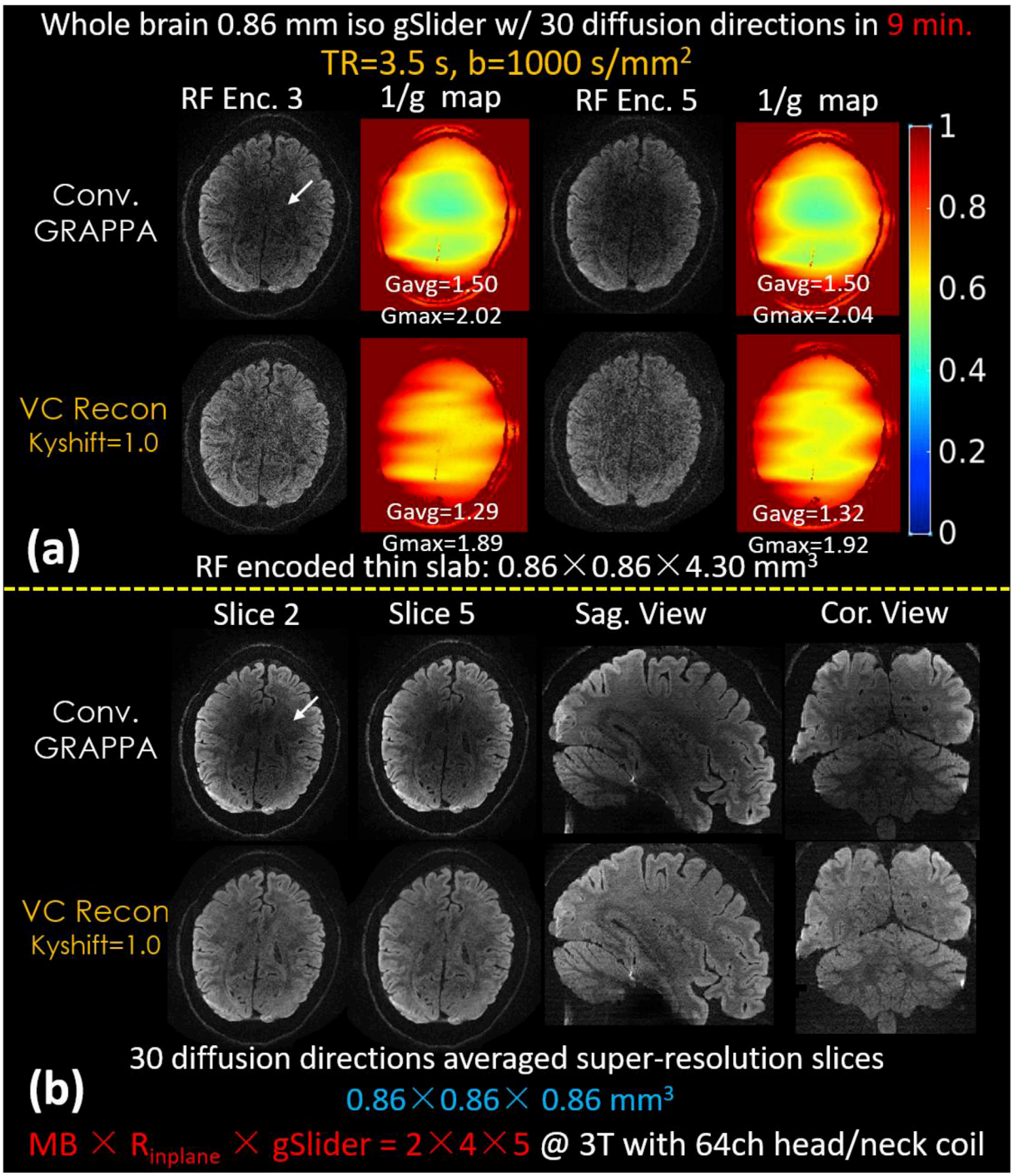

Fig. 9. Comparison of conventional and VC reconstructions for gSlider acquisition at 860 μm isotropic resolution ($R_{inplane} \times MB \times gSlider = 4 \times 2 \times 5$) with 30 diffusion-directions. (a) Reconstructed gSlider encoded thin-slabs at $0.86 \times 0.86 \times 4.3\ mm^3$ (2 out of 5 shown), and (b) final 30 diffusion-directions averaged 860 μm isotropic resolution reconstruction for two representative slices within the same slab. Sagittal and coronal views of averaged diffusion images are also shown in (b). VC reconstruction was able to improve the reconstruction performance while retaining structural differences that exist across the slices with each slab.

reconstruction through the proposed VC reconstruction, the residual artifacts are markedly reduced and hence the reduction in the striping artifacts.

A drawback in using VC-GRAPPA is the inability to employ partial *Fourier* in the acquisition which helps reduce TE and increase SNR. However, for high $R_{inplane}$ acquisitions, the SNR benefit from partial *Fourier* is relatively small and should be outweighed by the large reductions in reconstruction artifacts and the g-factor noise reduction afforded by VC-GRAPPA. For example, in the 1.5 mm isotropic acquisition used in this work, the imaging matrix size is 147 × 147 with a FOV of 220 mm. With $R_{inplane}$ of 3, there are 49 acquired k_y-lines and if partial *Fourier* of 6/8 were used then 12 k_y-lines before TE would have been skipped (at echo spacing of 0.65 ms). For the vendor provided monopolar acquisition used in this work, the reduction in TE from partial *Fourier* is 14 ms. For a representative brain tissue with T_2 of 70 ms, this TE reduction results in a SNR gain of $1/\left(e^{-\frac{14}{70}}\right) = 1.21x$, while the SNR loss of using a smaller acquisition window in partial *Fourier* is $\sqrt{6/8} = 0.86x$

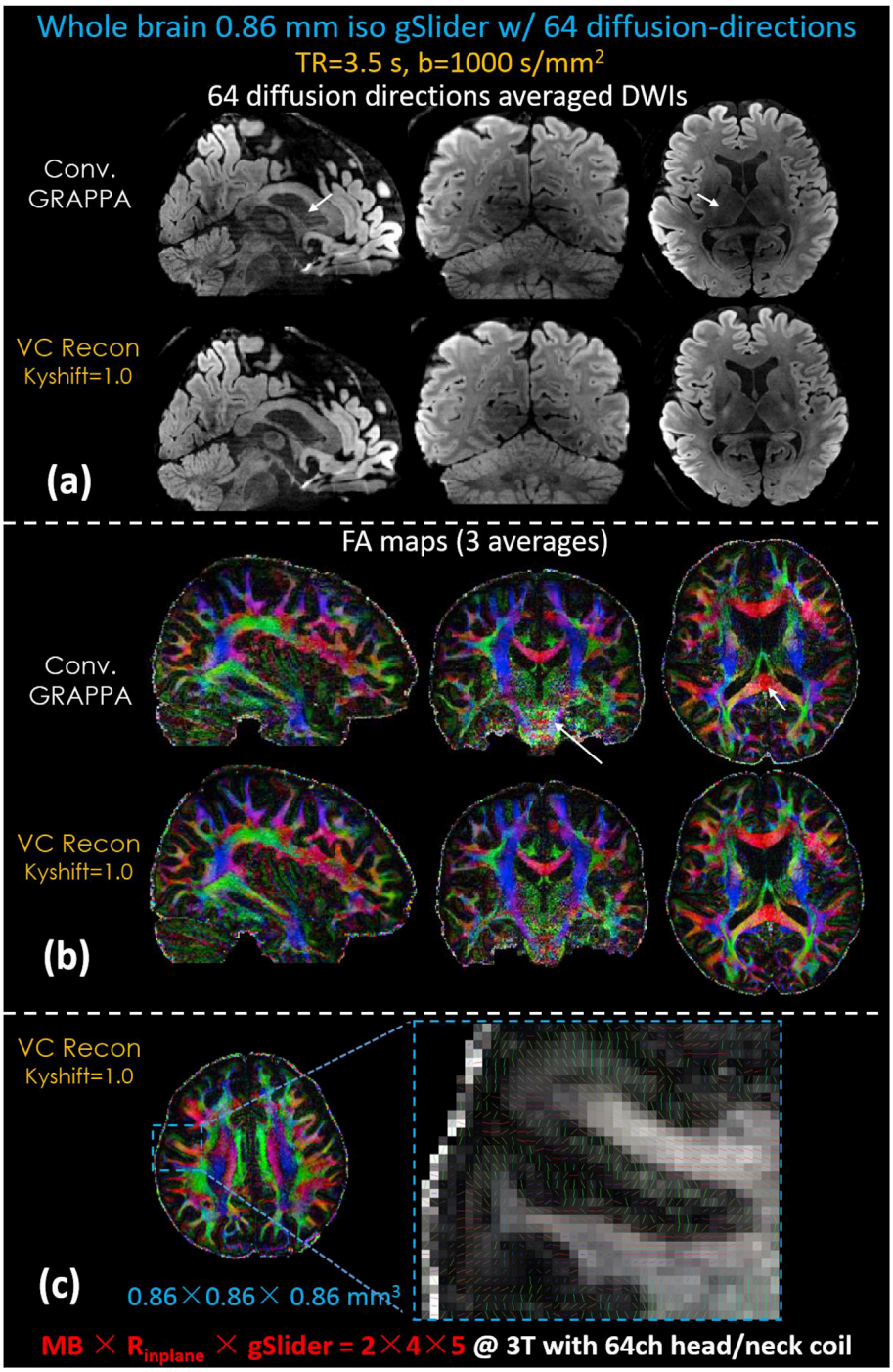

Fig. 10. Comparison of conventional and VC reconstructions of 860 μm isotropic resolution ($R_{inplane} \times MB \times gSlider = 4 \times 2 \times 5$) gSlider data with 64 diffusion-directions. (a) three views of 64 diffusion-directions averaged DWIs, and (b) FA maps. (c) The zoomed-in figure of the FA map obtained from VC reconstruction highlights the ability of the visualization of cortical diffusion pattern in this high resolution isotropic data.

for zero-filled and $\sqrt{3/5} = 0.77$x for homodyne reconstruction with ramp filter (Noll et al., 1991). This results in a net SNR factor of 1.04x and 0.93x respectively for the two partial *Fourier* reconstruction cases, showing that there is no net benefit in SNR from partial *Fourier* in this case. Moreover, without partial *Fourier*, VC coils can be used to provide ~20% g-factor noise reduction and provide a much better reconstruction with less artifacts and undesirable dark patches at the center of the image volume.

In this work, the $R_{inplane} \times MB = 3 \times 3$ acceleration acquisition is done to both reduce distortion and blurring ($R_{inplane} = 3$) as well as speed up the acquisition ($MB = 3$). To obtain higher SNR diffusion images, three averages of the acquisition are used. A comparison case at lower acceleration for this would therefore be that of an acquisition at $R_{inplane} = 3$ with matching distortion/blurring but with no MB acceleration. The mean g-factor for such acquisition is ~1.12. In comparing the SNR of a time-matched protocol of our 3×3 acquisition (3 averages) with the $R_{inplane} \times MB = 3 \times 1$ acquisition, the g-factor effect, the number of scan averages, and the differences in TR and hence T1 recovery (assuming the averaged T_1 in brain is 1000 ms) can be accounted for as follows:

$$SNR_{3\times3}^{3avgs}/SNR_{3\times1}^{1avg} = \sqrt{N_{average}}\cdot\frac{1-\exp(-TR_{3\times3}/T_1)}{1-\exp(-TR_{3\times1}/T_1)}\cdot\frac{1/gfactor_{3\times3}}{1/gfactor_{3\times1}}$$
$$= \sqrt{3}\cdot\frac{1-\exp(-3300/1000)}{1-\exp(-9900/1000)}\cdot\frac{1/1.22}{1/1.12}$$
$$= 1.53$$

As can be seen here, there are significant SNR benefits from the chosen acquisition compared to using a lower acceleration in a similar timespan. SMS encoding provides volumetric noise averaging, and hence SNR efficiency gain, which has lead to the observed 1.5x SNR benefit over the conventional 2D-EPI.

A phase matching process is proposed to correct the image phase of the reference data and enable VC reconstruction with correct phase prior. This was demonstrated to be important for high quality reconstruction. In the phase-matching process, a 2D Hamming filter was applied to mitigate the noise of the phase difference estimate between the conventionally reconstructed diffusion data and the reference data. There is a natural tradeoff in noise vs. artifact when selecting the k-space Hamming window size. A smaller window increases the amount of smoothing, which increases SNR of the reference data, but could also cost over-smoothing which can lead to inaccurate phase prior and aliasing artifacts in VC reconstruction. In this study, a window size of 20×20 was used to provide a good tradeoff in noise vs. artifact for the $b = 1000\ s/mm^2$ acquisitions. For diffusion data at higher b values where the SNR is low and there is a strong background phase variation, the selection of window size will need to be carefully tuned. The use of more sophisticated background phase estimation, such as through total variation (Eichner et al., 2015) could also be explored.

Another limitation of VC reconstruction is the increased reconstruction time. Currently the computation time of whole-brain 860 μm isotropic diffusion images with 64 diffusion directions using our prototypical offline VC-GRAPPA reconstruction in MATLAB is up to 30 h. The computation time of VC-GRAPPA is long because: (1) the data have to be reconstructed by GRAPPA to allow for background phase extraction, and then re-reconstructed by VC-GRAPPA with double the number of channels, which leads to longer computation time compared to standard reconstruction. (2) The GRAPPA weights need to be re-estimated to match the phase differences between diffusion and reference data TR-by-TR, which prolongs the reconstruction time. To reduce VC-GRAPPA reconstruction time, we now take advantage of parallel computing to achieve 10 h reconstruction time. We expect further shortening through coil compression and multi-core GPU computing (Wang et al., 2018b), which should allow for 1 h reconstruction time. With C++ and online reconstruction we expect further improvement which should allow this approach to be use in neuroscientific and clinical settings.

5. Conclusion

We introduce a phase-matched virtual-coil reconstruction framework with k_y & k_z shifted sampling strategy to improve the image quality of high resolution, highly accelerated SMS-EPI and gSlider-EPI acquisitions in diffusion imaging. In vivo studies demonstrated that the proposed method enables markedly improved reconstruction with reduced g-factor at high accelerations of 8–9 fold. The reduction in distortion and the improvement in acquisition speed achieved at these high accelerations should improve the quality of diffusion data that can be obtained in many clinical and neuroscience applications.

Acknowledgement

This work was supported in part by National Institutes of Health (NIH) research grants: R01EB020613, R01EB019437, R01MH116173, U01EB025162, P41EB015896, and the shared instrumentation grants: S10RR023401, S10RR019307, S10RR019254 and S10RR023043. This work was also partially supported by the National Natural Science Foundation of China (Grant No. 61871373 and No. 81729003), Strategic Priority Research Program of Chinese Academy of Sciences (Grant No. XDB25000000), Natural Science Foundation of Guangdong Province (Grant No. 2018A0303130132), Guangdong Provincial Key Laboratory of Magnetic Resonance and Multimodality Imaging (Grant No. 2014B030301013), Shenzhen Key Laboratory for MRI (Grant No. CXB201104220028A) and Shenzhen Key Laboratory of Ultrasound Imaging and Therapy (Grant No. ZDSYS20180206180631473).

References

Anderson, A.W., Gore, J.C., 1994. Analysis and correction of motion artifacts in diffusion weighted imaging. Magn. Reson. Med. 32, 379–387. https://doi.org/10.1002/mrm.1910320313.

Bammer, R., Keeling, S.L., Augustin, M., Pruessmann, K.P., Wolf, R., Stollberger, R., Hartung, H.P., Fazekas, F., 2001. Improved diffusion-weighted single-shot echo-planar imaging (EPI) in stroke using sensitivity encoding (SENSE). Magn. Reson. Med. 46, 548–554. https://doi.org/10.1002/mrm.1226.

Bilgic, B., Kim, T.H., Liao, C., Manhard, M.K., Wald, L.L., Haldar, J.P., Setsompop, K., 2018. Improving parallel imaging by jointly reconstructing multi-contrast data. Magn. Reson. Med. 80, 619–632. https://doi.org/10.1002/mrm.27076.

Blaimer, M., Breuer, F., Mueller, M., Heidemann, R.M., Griswold, M.A., Jakob, P.M., 2004. SMASH, SENSE, PILS, GRAPPA. How to choose the optimal method. Top. Magn. Reson. Imag. https://doi.org/10.1097/01.rmr.0000136558.09801.dd.

Blaimer, M., Choli, M., Jakob, P.M., Griswold, M.A., Breuer, F.A., 2013. Multiband phase-constrained parallel MRI. Magn. Reson. Med. 69, 974–980. https://doi.org/10.1002/mrm.24685.

Blaimer, M., Gutberlet, M., Kellman, P., Breuer, F.A., Köstler, H., Griswold, M.A., 2009. Virtual coil concept for improved parallel MRI employing conjugate symmetric signals. Magn. Reson. Med. 61, 93–102. https://doi.org/10.1002/mrm.21652.

Blaimer, M., Jakob, P.M., Breuer, F.A., 2014. Regularization method for phase-constrained parallel MRI. Magn. Reson. Med. 72, 166–171. https://doi.org/10.1002/mrm.24896.

Breuer, F.A., Kannengiesser, S.A.R., Blaimer, M., Seiberlich, N., Jakob, P.M., Griswold, M.A., 2009. General formulation for quantitative G-factor calculation in GRAPPA reconstructions. Magn. Reson. Med. 62, 739–746. https://doi.org/10.1002/mrm.22066.

Buehrer, M., Pruessmann, K.P., Boesiger, P., Kozerke, S., 2007. Array compression for MRI with large coil arrays. Magn. Reson. Med. 57, 1131–1139. https://doi.org/10.1002/mrm.21237.

Cauley, S.F., Polimeni, J.R., Bhat, H., Wald, L.L., Setsompop, K., 2014. Interslice leakage artifact reduction technique for simultaneous multislice acquisitions. Magn. Reson. Med. 72, 93–102. https://doi.org/10.1002/mrm.24898.

Chang, H.C., Guhaniyogi, S., Chen, N.K., 2015. Interleaved diffusion-weighted improved by adaptive partial-Fourier and multiband multiplexed sensitivity-encoding reconstruction. Magn. Reson. Med. 73, 1872–1884. https://doi.org/10.1002/mrm.25318.

Chen, N. kuei, Guidon, A., Chang, H.C., Song, A.W., 2013. A robust multi-shot scan strategy for high-resolution diffusion weighted MRI enabled by multiplexed sensitivity-encoding (MUSE). Neuroimage 72, 41–47. https://doi.org/10.1016/j.neuroimage.2013.01.038.

Constable, R.T., Gore, J.C., 1992. The loss of small objects in variable TE imaging: implications for FSE, RARE, and EPI. Magn. Reson. Med. 28, 9–24. https://doi.org/10.1002/mrm.1910280103.

Cuppen, J., van Est, A., 1987. Reducing MR imaging time by one-sided reconstruction. Magn. Reson. Imaging 5, 526–527. https://doi.org/10.1016/0730-725X(87)90402-4.

Dai, E., Ma, X., Zhang, Z., Yuan, C., Guo, H., 2017. Simultaneous multislice accelerated interleaved EPI DWI using generalized blipped-CAIPI acquisition and 3D K-space reconstruction. Magn. Reson. Med. 77, 1593–1605. https://doi.org/10.1002/mrm.26249.

Eichner, C., Cauley, S.F., Cohen-Adad, J., Möller, H.E., Turner, R., Setsompop, K., Wald, L.L., 2015. Real diffusion-weighted MRI enabling true signal averaging and increased diffusion contrast. Neuroimage 122, 373–384. https://doi.org/10.1016/j.neuroimage.2015.07.074.

Fan, Q., Nummenmaa, A., Polimeni, J.R., Witzel, T., Huang, S.Y., Wedeen, V.J., Rosen, B.R., Wald, L.L., 2017. HIgh b-value and high Resolution Integrated Diffusion (HIBRID) imaging. Neuroimage 150, 162–176. https://doi.org/10.1016/j.neuroimage.2017.02.002.

Gao, H., Li, L., Zhang, K., Zhou, W., Hu, X., 2014. PCLR: phase-constrained low-rank model for compressive diffusion-weighted MRI. Magn. Reson. Med. 72, 1330–1341. https://doi.org/10.1002/mrm.25052.

Griswold, M.A., Jakob, P.M., Heidemann, R.M., Nittka, M., Jellus, V., Wang, J., Kiefer, B., Haase, A., 2002. Generalized autocalibrating partially parallel acquisitions (GRAPPA). Magn. Reson. Med. 47, 1202–1210. https://doi.org/10.1002/mrm.10171.

Guo, H., Ma, X., Zhang, Z., Zhang, B., Yuan, C., Huang, F., 2016. POCS-enhanced inherent correction of motion-induced phase errors (POCS-ICE) for high-resolution multishot diffusion MRI. Magn. Reson. Med. 75, 169–180. https://doi.org/10.1002/mrm.25594.

Haacke, E.M., Lindskogj, E.D., Lin, W., 1991. A fast, iterative, partial-fourier technique capable of local phase recovery. J. Magn. Reson. 92, 126–145. https://doi.org/10.1016/0022-2364(91)90253-P.

Haldar, J.P., 2014. Low-rank modeling of local k-space neighborhoods (LORAKS) for constrained MRI. IEEE Trans. Med. Imag. 33, 668–681. https://doi.org/10.1109/TMI.2013.2293974.

Haldar, J.P., Wedeen, V.J., Nezamzadeh, M., Dai, G., Weiner, M.W., Schuff, N., Liang, Z.-P., 2013. Improved diffusion imaging through SNR-enhancing joint reconstruction. Magn. Reson. Med. 69, 277–289. https://doi.org/10.1002/mrm.24229.

Hu, Y., Levine, E.G., Tian, Q., Moran, C.J., Wang, X., Taviani, V., Vasanawala, S.S., McNab, J.A., Daniel, B.A., Hargreaves, B.L., 2018. Motion-robust reconstruction of multishot diffusion-weighted images without phase estimation through locally low-rank regularization. Magn. Reson. Med. https://doi.org/10.1002/mrm.27488.

Hu, Z., Ma, X., Truong, T.K., Song, A.W., Guo, H., 2017. Phase-updated regularized SENSE for navigator-free multishot diffusion imaging. Magn. Reson. Med. 78, 172–181. https://doi.org/10.1002/mrm.26361.

Jenkinson, M., Beckmann, C.F., Behrens, T.E.J., Woolrich, M.W., Smith, S.M., 2012. Fsl. Neuroimage. https://doi.org/10.1016/j.neuroimage.2011.09.015.

Jeong, H.K., Gore, J.C., Anderson, A.W., 2013. High-resolution human diffusion tensor imaging using 2-D navigated multishot SENSE EPI at 7 T. Magn. Reson. Med. 69, 793–802. https://doi.org/10.1002/mrm.24320.

Kettinger, A.O., Kannengiesser, S.A.R., Breuer, F.A., Vidnyanszky, Z., Blaimer, M., 2018. Controlling the object phase for g-factor reduction in phase-Constrained parallel MRI using spatially selective RF pulses. Magn. Reson. Med. 79, 2113–2125. https://doi.org/10.1002/mrm.26890.

Liao, C., Chen, Y., Cao, X., Chen, S., He, H., Mani, M., Jacob, M., Magnotta, V., Zhong, J., 2017. Efficient parallel reconstruction for high resolution multishot spiral diffusion data with low rank constraint. Magn. Reson. Med. 77, 1359–1366. https://doi.org/10.1002/mrm.26199.

Liao, C., Stockmann, J., Tian, Q., Bilgic, B., Manhard, M.K., Wald, L.L., Setsompop, K., 2018. High-fidelity, High-Isotropic Resolution Diffusion Imaging through gSlider Acquisition with B1+ & T1 Corrections and Multi-Coil B0 Shim Array arXiv preprint. 1811.05473.

Mani, M., Jacob, M., Guidon, A., Magnotta, V., Zhong, J., 2015. Acceleration of high angular and spatial resolution diffusion imaging using compressed sensing with multichannel spiral data. Magn. Reson. Med. 73, 126–138. https://doi.org/10.1002/mrm.25119.

Mani, M., Jacob, M., Kelley, D., Magnotta, V., 2017. Multi-shot sensitivity-encoded diffusion data recovery using structured low-rank matrix completion (MUSSELS). Magn. Reson. Med. 78, 494–507. https://doi.org/10.1002/mrm.26382.

Noll, D.C., Nishimura, D.G., Macovski, A., 1991. Homodyne detection in magnetic resonance imaging. IEEE Trans. Med. Imag. 10, 154–163. https://doi.org/10.1109/42.79473.

Polimeni, J.R., Bhat, H., Witzel, T., Benner, T., Feiweier, T., Inati, S.J., Renvall, V., Heberlein, K., Wald, L.L., 2016. Reducing sensitivity losses due to respiration and motion in accelerated echo planar imaging by reordering the autocalibration data acquisition. Magn. Reson. Med. 75, 665–679. https://doi.org/10.1002/mrm.25628.

Porter, D.A., Heidemann, R.M., 2009. High resolution diffusion-weighted imaging using readout-segmented echo-planar imaging, parallel imaging and a two-dimensional navigator-based reacquisition. Magn. Reson. Med. 62, 468–475. https://doi.org/10.1002/mrm.22024.

Schneider, J.T., Blaimer, M., Ullmann, P., 2012. Tailoring the image background phase by spatially selective excitation for improved parallel imaging reconstruction performance. In: Proceedings of the 20th Annual Meeting of ISMRM, Melbourne, Australia, p. 516.

Setsompop, K., Cohen-Adad, J., Gagoski, B.A., Raij, T., Yendiki, A., Keil, B., Wedeen, V.J., Wald, L.L., 2012a. Improving diffusion MRI using simultaneous multi-slice echo planar imaging. Neuroimage 63, 569–580. https://doi.org/10.1016/j.neuroimage.2012.06.033.

Setsompop, K., Fan, Q., Stockmann, J., Bilgic, B., Huang, S., Cauley, S.F., Nummenmaa, A., Wang, F., Rathi, Y., Witzel, T., Wald, L.L., 2018. High-resolution in vivo diffusion imaging of the human brain with generalized slice dithered enhanced resolution: simultaneous multislice (gSlider-SMS). Magn. Reson. Med. 79, 141–151. https://doi.org/10.1002/mrm.26653.

Setsompop, K., Gagoski, B.A., Polimeni, J.R., Witzel, T., Wedeen, V.J., Wald, L.L., 2012b. Blipped-controlled aliasing in parallel imaging for simultaneous multislice echo planar imaging with reduced g-factor penalty. Magn. Reson. Med. 67, 1210–1224. https://doi.org/10.1002/mrm.23097.

Shi, X., Ma, X., Wu, W., Huang, F., Yuan, C., Guo, H., 2015. Parallel imaging and compressed sensing combined framework for accelerating high-resolution diffusion tensor imaging using inter-image correlation. Magn. Reson. Med. 73, 1775–1785. https://doi.org/10.1002/mrm.25290.

Wang, F., Bilgic, B., Dong, Z., Manhard, M.K., Ohringer, N., Zhao, B., Haskell, M., Cauley, S.F., Fan, Q., Witzel, T., Adalsteinsson, E., Wald, L.L., Setsompop, K., 2018a. Motion-robust sub-millimeter isotropic diffusion imaging through motion corrected generalized slice dithered enhanced resolution (MC-gSlider) acquisition. Magn. Reson. Med. 80, 1891–1906. https://doi.org/10.1002/mrm.27196.

Wang, H., Peng, H., Chang, Y., Liang, D., 2018b. A survey of GPU-based acceleration techniques in MRI reconstructions. Quant. Imag. Med. Surg. 8, 196–208. https://doi.org/10.21037/qims.2018.03.07.

Wang, H., Polimeni, J.R., Bilgic, B., Wald, L.L., Setsompop, K., 2017. Analytical G-factor calculation for slice-GRAPPA with dual "Even-Odd" kernels (SG-DK). Proc. Int. Soc. Magn. Reson. Med. 25, 5159.

Wang, J., Zhang, B., Zhong, K., Zhuo, Y., 2005. Image domain based fast GRAPPA reconstruction and relative SNR degradation factor image domain GRAPPA algorithm. In: Proceedings of the 13th Annual Meeting of ISMRM. Miami, p. 2428.

Wen, Q., Kodiweera, C., Dale, B.M., Shivraman, G., Wu, Y.C., 2018. Rotating single-shot acquisition (RoSA) with composite reconstruction for fast high-resolution diffusion imaging. Magn. Reson. Med. 79, 264–275. https://doi.org/10.1002/mrm.26671.

Xie, V.B., Lyu, M., Liu, Y., Feng, Y., Wu, E.X., 2018. Robust EPI Nyquist ghost removal by incorporating phase error correction with sensitivity encoding (PEC-SENSE). Magn. Reson. Med. 79, 943–951. https://doi.org/10.1002/mrm.26710.

Zhang, Z., Huang, F., Ma, X., Xie, S., Guo, H., 2015. Self-feeding MUSE: a robust method for high resolution diffusion imaging using interleaved EPI. Neuroimage 105, 552–560. https://doi.org/10.1016/j.neuroimage.2014.10.022.